Hydrogeology Journal (2021) 29:331–345
https://doi.org/10.1007/s10040-020-02252-5

PAPER

Comparisons on the effects of temperature, runoff, and land-cover on carbonate weathering in different karst catchments: insights into the future global carbon cycle

Sibo Zeng[1] · Zaihua Liu[2,3] · Nico Goldscheider[4] · Simon Frank[4] · Nadine Goeppert[4] · Georg Kaufmann[1] · Cheng Zeng[2] · Qingrui Zeng[2] · Hailong Sun[2]

Received: 23 April 2020 / Accepted: 30 September 2020 / Published online: 10 October 2020

Abstract

This study compares and analyzes high-frequency hydrochemical data from three karst catchments in the mountainous Gadenalpe (GAC, Austrian Alps), Tsanfleuron-Sanetsch (TSC, Swiss Alps), and Banzhai (BZC, SW China) regions, to differentiate the effects of temperature, runoff, and land-cover on carbonate weathering. The results show that when bare rock dominates in the recharge area, as in the GAC and TSC, the seasonal discharge variations account for the most significant change in HCO_3^- concentration. In these two alpine catchments, maximum HCO_3^- concentrations occurred in the cold season when the areas were covered by snow and discharge was low, whereas minimum HCO_3^- concentrations occurred in the warm season, when snowmelt and/or glacier melt caused higher discharge and dilution. In contrast, control by the strong seasonal variation in soil respiration in the subtropical catchment (BZC), caused by the well-developed forest cover, exceeded the negative impact of temperature on carbonate weathering. This led to higher HCO_3^- concentrations during the summer growing season than in the winter dormant season. This study demonstrates that the occurrence of different soils/vegetation has a profound impact on the behavior of carbonate weathering on land, from negative temperature- and discharge-driven correlations in alpine catchments to positive soil CO_2-driven correlation in subtropical catchments. Based on the equilibrium modeling of HCO_3^- concentration for a global temperature range, it is predicted that under future global warming, karst regions in cold climates with vegetation cover will have increasing CO_2 consumption potential, whereas karst regions in warm climates will have decreasing CO_2 consumption potential.

Keywords Karst · Carbonate weathering · Climate change · Land-cover (CO_2) effect · Global carbon cycle

Published in the special issue "Five decades of advances in karst hydrogeology".

✉ Sibo Zeng
sibozeng@zedat.fu-berlin.de

✉ Zaihua Liu
liuzaihua@vip.gyig.ac.cn

✉ Nico Goldscheider
nico.goldscheider@kit.edu

[1] Institute of Geological Sciences, Geophysics Section, Freie Universität Berlin, 12249 Berlin, Germany

[2] State Key Laboratory of Environmental Geochemistry (SKLEG), Institute of Geochemistry, Chinese Academy of Sciences (CAS), Guiyang 550081, Guizhou, China

[3] CAS Center for Excellence in Quaternary Science and Global Change, 710061, Xi'an, China

[4] Institute of Applied Geosciences, Division of Hydrogeology, Karlsruhe Institute of Technology (KIT), 76131 Karlsruhe, Germany

Introduction

Over the past few decades, evidence has emerged of an increased continental chemical weathering flux (indicated by bicarbonate flux, e.g., Raymond et al. 2008; Gislason et al. 2009; Macpherson et al. 2019). It has generally been suggested that ongoing global climate change accounts for most of the increased weathering flux. Bicarbonate (HCO_3^-) is the main form of dissolved inorganic carbon (DIC) in natural waters with an alkaline pH range from 7 to 9 (Dreybrodt 1988). The riverine HCO_3^- flux generated by carbonate weathering from karst terrains is an important component of the terrestrial carbon cycle (e.g., Liu and Zhao 2000; Zeng et al. 2019). It can enhance aquatic photosynthesis and buffer the pH in both freshwater and oceans (Riebesell et al. 2007; Liu et al. 2010, Liu et al. 2018).

A growing body of evidence suggests that terrestrial carbonate weathering depends on both natural and anthropogenic factors (Dreybrodt 1988. Martin, 2017; Raymond and Hamilton. 2018; Zeng et al. 2019). The much faster chemical weathering kinetics of carbonates compared with silicates makes carbonates more sensitive in their responses to such environmental fluctuations (Liu et al. 2011; Beaulieu et al. 2012; Zeng et al. 2019). Because of the global distribution of carbonate rocks (~15% of the global ice-free continental surface is characterized by the presence of karstifiable carbonate rock, Goldscheider et al. 2020) and an even larger area covered by soils with carbonate minerals (Adams and Post 1999), this feedback may cause considerable carbon sink flux variations in the future, which may play a significant role in the global carbon cycle (Liu et al. 2010, 2018; Zeng et al. 2019).

Because of the complexity of the process forming DIC, estimating the general feedback of carbonate-weathering carbon sink flux (CCSF) associated with both ongoing climate change and human forcing is still an unresolved task for the geochemical community. The CCSF is controlled by both physicochemical and ecological drivers, including temperature (Gaillardet et al. 2019; Romero-Mujalli et al. 2019a), precipitation/runoff (Zeng et al. 2012, 2016), net primary production (Goddéris et al. 2010), land cover types (Zeng et al. 2017, 2019), and soil water content (Romero-Mujalli et al. 2019b). Under natural conditions, all of these factors might closely interact (Beaulieu et al. 2012). However, the main drivers of CCSF differ from place to place; therefore, to date, it has been difficult to quantify or predict the future DIC flux using the limited knowledge.

Generally, temperature is a fundamental controlling factor for carbonate weathering, and has been studied extensively. The most significant barrier for understanding carbonate weathering behavior is the multiple roles of temperature in determining the solubility of carbonate rocks. First, the thermodynamics of chemical weathering shows a lower solubility of carbonates as the temperature increases (Dreybrodt 1988); however, the temperature may be related to ecological drivers such as the CO_2 in the root zone (Gwiazda and Broecker 1994; Gaillardet et al. 2019; Romero-Mujalli et al. 2019a). The DIC concentration may show a "bell-shape" relationship with temperature (Gaillardet et al. 2019), which may be related to the ecosystem where soil CO_2 is produced in the root zone by soil biota. In addition, according to Gwiazda and Broecker (1994), land use also has a great impact on soil respiration. A recent simulation test showed that grassland, shrubland, cropland, bare soil, and bare rock follow a decreasing DIC concentration sequence because of their different soil CO_2 contents (Zeng et al. 2017). Indeed, primary production and soil respiration may differ from species to species and show diverse sensitivities to specific climatic drivers (Del Grosso et al. 2008; Bond-Lamberty and Thomson 2010; Hibbard et al. 2005; Thomey et al. 2011). Moreover, land-use conversion may lead to substantial changes in primary production and soil respiration by altering cover types and soil properties (Haberl et al. 2007; Sheng et al. 2010). Therefore, a unified equation for estimating the global DIC concentration based on climatic parameters alone may neglect the roles of land use and land cover (Zeng et al. 2019).

To reach a better understanding of the carbonate weathering processes under different land covers, this study compares and analyzes high-frequency hydrochemical data from a recent study site at the Gadenalpe catchment (GAC, in the Austrian Alps; S. Frank et al., Karlsruhe Institute of Technology (Germany), unpublished paper, 2020) and two previous studies at the Tsanfleuron-Sanetsch catchment (TSC, Swiss Alps; Zeng et al. 2012) and Banzhai Catchment (BZC, SW China; Zeng et al. 2016). The existing studies addressed individual examples, in which dilution effects and dominance of runoff in CCSF were found, but the temperature effect related to the thermodynamics of carbonate dissolution (Dreybrodt 1988) and the CO_2 effect related to land cover (Dreybrodt 1988; Liu et al. 2007) remain to be examined. The added value of this study is a systematic comparison that allows differentiation of the effects of temperature, runoff, and land-cover on carbonate weathering.

Study sites

Gadenalpe catchment (GAC)

The Gadenalpe catchment (GAC) is located in the eastern Alps, western Austria, and has a total drainage area of nearly 7 km^2 (Fig. 1; S. Frank et al., Karlsruhe Institute of Technology, unpublished paper, 2020). Geomorphologically, the catchment is a typical alpine cirque with an average elevation of about 2,100 m. The lithology is dominated by the Hauptdolomit-Plattenkalk Formation consisting of Triassic dolostone and limestone. The total discharge of the aquifer is mainly drained via a karst spring at the bottom of the cirque (Fig. 1b). The hydrological pattern in the GAC can be divided into three distinct periods: freezing and snow cover (about December–April), snowmelt (May–June), and a long season characterized by highly variable conditions (mixture of very rainy and dry periods; July–November). As shown in Fig. 1b, bare rock is the main land cover in the elevated parts of the GAC, covering 64% of the area, whereas grass, shrubs, and forest are present at lower elevations close to the spring outlet, and cover nearly 36% of the area (S. Frank

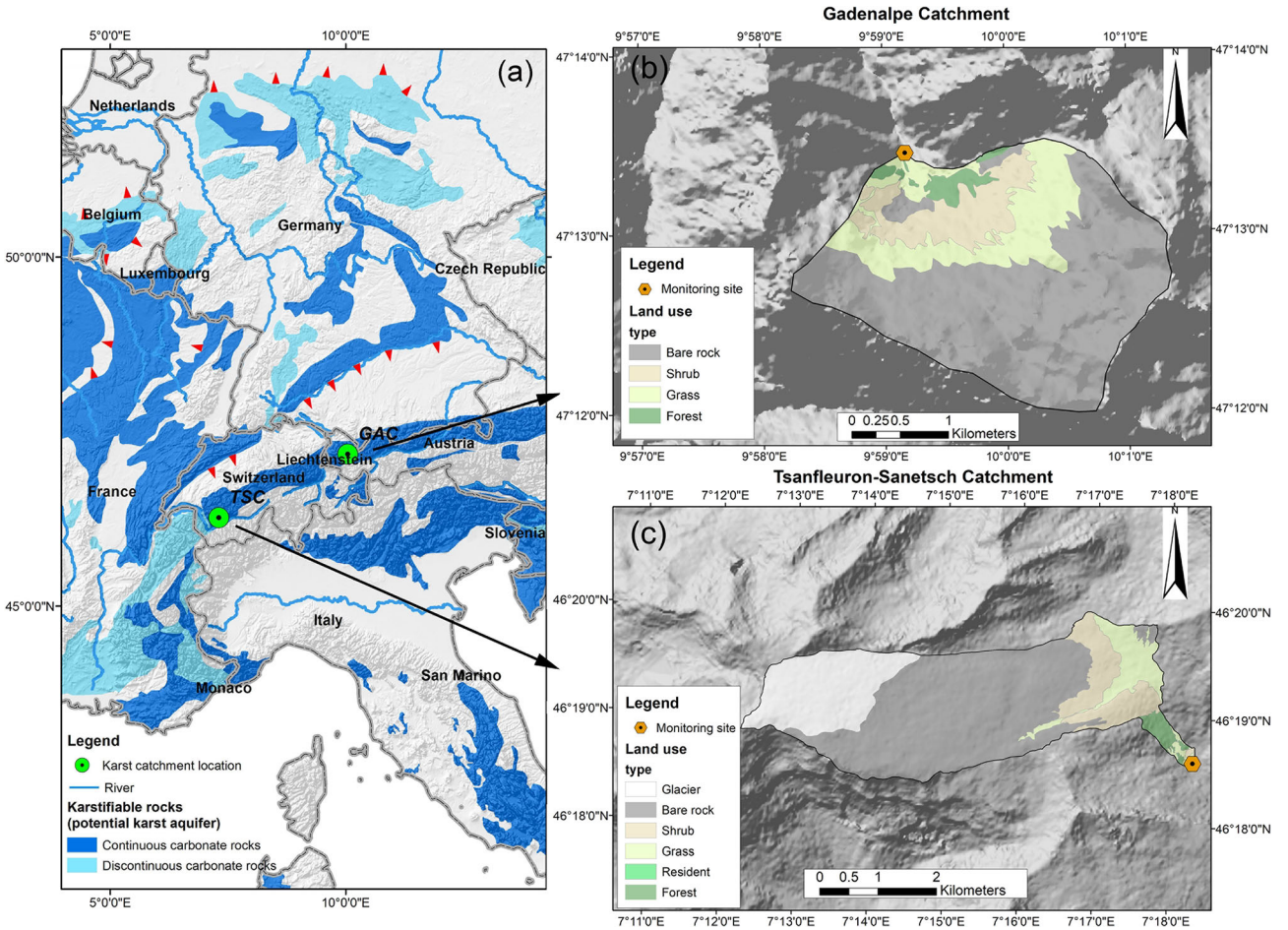

Fig. 1 **a** Locations of the two alpine karst catchments, shown on the World Karst Aquifer Map (Goldscheider et al. 2020); topography and land use of **b** the Gadenalpe Catchment (GAC, S. Frank et al., Karlsruhe Institute of Technology, unpublished paper, 2020) and **c** the Tsanfleuron-Sanetsch Catchment (TSC, Gremaud et al. 2009). The land use/land cover in the GAC has been classified based on contemporaneous remote-sensing images. The spring outlet (monitoring site) is highlighted with an orange hexagon (note: the monitoring site for the GAC is ~200–300 m from the spring outlet because of the inaccessibility of the outlet)

et al., Karlsruhe Institute of Technology, unpublished paper, 2020).

Tsanfleuron-Sanetsch catchment (TSC)

The Tsanfleuron-Sanetsch catchment (TSC) is approximately 11 km^2 in size and belongs to the Helvetic domain of the Swiss Alps (Fig. 1). The rapidly retreating Tsanfleuron Glacier is at the highest part of the area, from 2,550 to 3,000 m in elevation. The catchment area experiences both a temperate continental climate and a mountain climate with pronounced precipitation and seasonal snow. Geologically, two limestone formations (Urgonian–Eocene) form one hydraulically connected karst aquifer in the area. The total discharge of the aquifer is mainly drained via Glarey Spring at an elevation of 1,553 m (Gremaud et al. 2009; Gremaud and Goldscheider 2010). According to the previous study undertaken by the authors (S. Frank et al., Karlsruhe Institute of Technology, unpublished paper, 2020), the discharge patterns in the TSC can be divided into three hydrological periods: the freezing season, the snow-melting season, and the glacier-melting season (Zeng et al. 2012). The freezing season or snow-cover period typically lasts from December to April, followed by the snow-melting period from May to June. By mid-July, the snowline reaches the glacier front and the melting glacier sustains the water flow until November or December, even during long dry periods. During the snow- and glacier-melting seasons, rainfall events cause additional discharge peaks at shorter time scales. Inside the catchment, the glacier and bare rock constitute the largest portion of the land surface (~80%). The area close to the catchment outlet is covered by natural vegetation such as forest, grass, and shrubs (Fig. 1c).

Banzhai catchment (BZC)

The Banzhai catchment (BZC) is located in Libo County, Guizhou Province, Southwest China (Fig. 2). The drainage

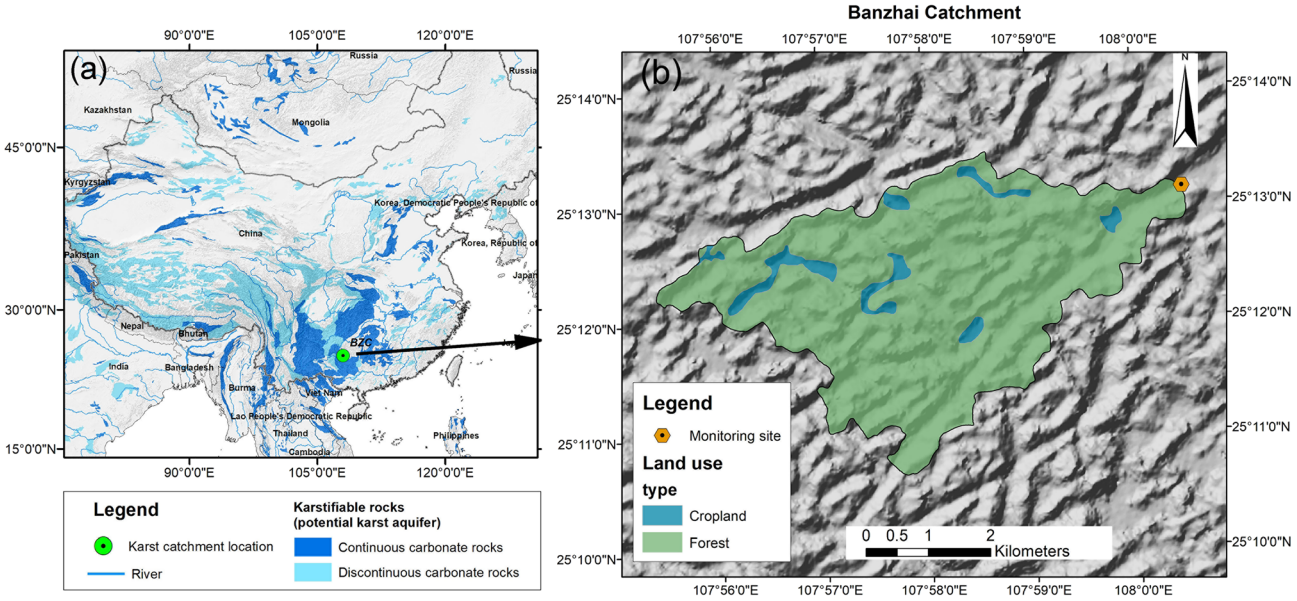

Fig. 2 **a** Location of the Banzai Catchment (BZC) shown on the World Karst Aquifer Map (Goldscheider et al. 2020); **b** topography and land use of BZC (Zeng et al. 2016). The land use/land cover in the BZC has been classified based on contemporaneous remote-sensing images. Natural forest dominates 95% of the total area, followed by a smaller area of cropland (~5%). The spring outlet (sensor location) is highlighted with an orange hexagon

area of the BZC is geomorphologically a typical karst peak cluster, approximately 19 km^2 in size (Zeng et al. 2016). Because of the strong impacts of the Asian monsoon in summer, the precipitation here mostly falls between April and September, during a period of higher temperature and greater moisture. The main lithology is dolomitic limestone of Middle and Lower Carboniferous age. As shown in Fig. 2b, a natural forest dominates most of the land surface (95%), followed by a small proportion of cropland (5%). A thin soil layer covers most of the land surface with a thickness of 0–20 cm. The hydrological patterns in the BZC can be separated into the monsoon season in spring–summer and the dry season in autumn–winter. Major storm events occur in the hot summer, leading to higher discharge at the same time.

Methods

Automatic logging of high-resolution physicochemical data

A CTDP300 multi-parameter water quality meter (Greenspan Corporation, Australia) and an OTT CTD logger (water level and specific electrical conductivity (EC), Ott HydroMet, Kempten, Germany) were set up near or at the spring outlets in the BZC and GAC from 2009 to 2011 (Zeng et al. 2016) and 2017 to 2019 (S. Frank et al., Karlsruhe Institute of Technology, unpublished paper, 2020), respectively. In the GAC, the spring consists of several outlets that are inaccessible for sampling; therefore, the measurement station was installed 200–300 m downstream of the individual outlets, which also means that water temperature at this site was influenced by air temperature. Stage–discharge curves were acquired by flow measurements using the salt-dilution method. The CTDP300 sensor continuously recorded physicochemical parameters, including water temperature, water stage, pH, and EC, with resolutions of 0.01 °C, 0.01 m, 0.01 unit, and 0.1 µS/cm, respectively. A WTW 350i hand-held water quality meter (WTW Company, Germany) was used to check the reliability of the automatically logged CTDP300 sensor data during field visits (S. Frank et al., Karlsruhe Institute of Technology, unpublished paper, 2020).

Discharge of Glarey Spring in the TSC was recorded by an ultrasonic water-level device and a pressure probe at the overflow spring. The stage–discharge curves were acquired by flow measurements using the salt-dilution method. Additionally, EC, pH, and water temperature sensors were installed at Glarey Spring. Water temperature and EC were measured using a field conductivity probe (WTW 340i, Weilheim, Germany) with resolutions of 0.1 °C and 0.5 µS/cm, respectively. The pH was recorded by a pH probe (WQ201, Global Water Instrumentation, Gold River, California, USA) and a data logger (DT50, DataTaker, Orbatex, Grenchen, Switzerland) with a resolution of 0.1 unit (Gremaud et al. 2009; Zeng et al. 2012).

Meteorological data

In the GAC, meteorological data, including hourly air temperature and precipitation data with a temporal resolution of

15 min, were gathered from the nearby automatic meteorological station located in Sonntag/Stein, Austria. A tipping-bucket rain gauge with a temporal resolution of 30 min was installed near the eastern margin of the TSC at an elevation 2,120 m (Gremaud et al. 2009). The daily air temperature and precipitation data in the BZC were collected from the state meteorological station in Libo County (Zeng et al. 2016).

In-situ titration and major ion analyses

Aquamerck alkalinity and hardness test kits were used to determine the HCO_3^- and Ca^{2+} concentrations by in-situ titration in the field, with accuracies of 0.05 mmol L^{-1} and 1 mg L^{-1}, respectively. The water sampled in the field was filtered through a 0.45-μm Millipore filter into acid- and purified water-washed plastic bottles for later analysis of major cations and anions in the laboratory. The water samples for the cation test were acidified to pH <2 by nitric acid in situ to prevent $CaCO_3$ precipitation. Major ions in the water samples were tested in the laboratory.

In 2016, 40 water samples were collected at the GAC spring and analyzed in the laboratory of the Karlsruhe Institute of Technology (KIT)—Faust (2017); S. Frank et al., Karlsruhe Institute of Technology, unpublished paper, 2020). The sampling frequency of the spring water was every 2 months in the BZC from 2009 to 2011 (Zeng et al. 2016). In the laboratory of the State Key Laboratory of Environmental Geochemistry (SKLEG), the concentrations of Na^+, K^+, and Mg^{2+} in the BZC samples were determined by inductively coupled plasma-optical emission spectrometry (ICP-OES). The Ca^{2+} concentrations were also tested by ICP-OES to verify the in-situ titration field test results. Concentrations of SO_4^{2-} and Cl^- were determined by ion chromatography (Dionex ICS-90). In the TSC, the major cation and anion tests of 162 water samples from Glarey Spring were performed by ion chromatography (IC, Dionex DX-120) at the Centre for Hydrogeology and Geothermics at the University of Neuchatel (CHYN) laboratory; the tested ions included K^+, Na^+, Ca^{2+}, Mg^{2+}, Cl^-, NO_3^-, SO_4^{2-}, and HCO_3^- (Zeng et al. 2012).

Calculation of continuous HCO_3^- concentration, water pCO_2, SI_c, and SI_d

The high-resolution measurements of bicarbonate concentration in water is significant for detecting the dynamics of carbonate weathering response to environmental drivers. In the GAC, BZC, and TSC, the dominant lithology is carbonate rock, limestone and/or dolomite. The water EC was affected by Ca^{2+}, Mg^{2+}, and HCO_3^-, the dominant ions in the solutions. In these catchments, simple linear regression was used between EC and the concentrations of the different species, HCO_3^-, Ca^{2+}, and Mg^{2+}, separately. From these three regression functions, the continuous concentrations of HCO_3^-, Ca^{2+}, and Mg^{2+} (S. Frank et al., Karlsruhe Institute of Technology, unpublished paper, 2020; Zeng et al. 2012, 2016) were estimated. In addition, the water CO_2 partial pressure (pCO_2) and calcite or dolomite saturation index (SI_c or SI_d) were calculated based on the concentrations of K^+, Na^+, Ca^{2+}, Mg^{2+}, Cl^-, SO_4^{2-}, and HCO_3^-, as well as pH and water temperature (Liu et al. 2007; Zeng et al. 2016). Here, the geochemical program WATSPEC (Wigley 1977) was used to calculate the water pCO_2, SI_c, and SI_d using the continuous logged or calculated water temperature, pH, and concentrations of Ca^{2+}, Mg^{2+}, and HCO_3^- from the three catchments.

Calculation of carbonate-weathering carbon sink flux

The CCSF can be calculated by following the standard equation (e.g. Liu et al. 2010; Zeng et al. 2019):

$$\mathrm{CCSF} = 0.5 \cdot M_{(\mathrm{C})} \cdot h \cdot \left[\mathrm{HCO_3^-}\right] \quad (1)$$

where CCSF is in t C km^{-2} $year^{-1}$, h is the runoff depth of the catchment in m $year^{-1}$, $[HCO_3^-]$ is the actual concentration of bicarbonate in mmol L^{-1}, and $M_{(C)}$ is the molar mass of carbon in g/mol. The factor 0.5 is a conversion factor implying that only half of the HCO_3^- flux originates from atmospheric and/or soil CO_2 (i.e., carbon sink), whereas the other half is from the dissolution of carbonate minerals.

Results

Seasonal variations in physicochemical parameters and CCSF

Figure 3 shows the nearly 2-year synchronous high-resolution measurements of the meteorological parameters, air temperature and precipitation, and spring water physicochemical parameters, water temperature, pH, and discharge. The calculated parameters in the GAC, BZC and TSC, $[HCO_3^-]$, pCO_2, SI_c, SI_d, and CCSF, are also shown here.

All of these catchments presented distinct seasonal variations in air temperature of ~30 °C between summer and winter, with a similar range with respect to amplitude. In the GAC (Fig. 3a) and BZC (Fig. 3b), the measured water temperatures peaked between July and August, whereas minimum values occurred between January and March. The seasonal fluctuation of the water temperature in the GAC was approximately 10 °C, which shows the direct impact of air temperature at this measurement site (as described previously). In the BZC, the seasonal variation in water temperature was ~2 °C. The average spring water temperature in the TSC showed no significant seasonal variation during the study period, with an almost constant value of around 4 ± 0.5 °C (Fig. 3c).

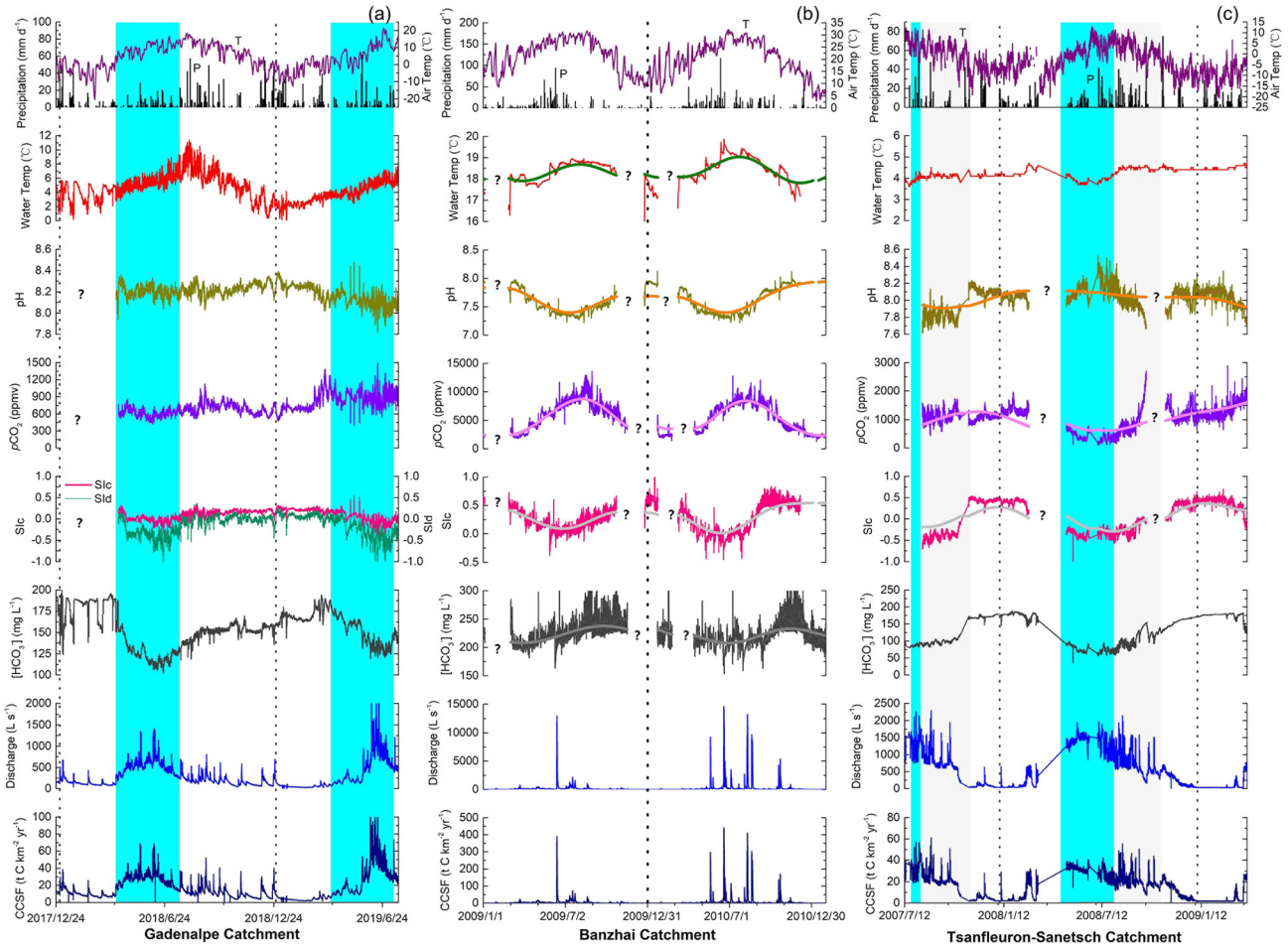

Fig. 3 Seasonal variations in air temperature, precipitation, water temperature, discharge, pH, calculated pCO_2, calcite and dolomite saturation indices (SI_c, SI_d), concentrations of HCO_3^- (the main form of DIC), and carbonate-weathering carbon sink flux (CCSF) in **a** the Gadenalpe Catchment (GAC), **b** the Banzhai Catchment (BZC), and **c** the Tsanfleuron-Sanetsch Catchment (TSC). The blue shaded areas mark the snow-melting periods, and the gray-shaded areas indicate glacier-melting periods. The dashed lines separate years (January 1). Note: The water temperature variations in the GAC are an artifact, because the measurement point is about 200–300 m below the spring outlets due to inaccessibility of the outlets. There are most likely no relevant water temperature variations at the spring because the carbonate rock aquifer is very thick. ?: data gap due to a technical or calibration problem

The average spring water pCO_2 in the BZC was the highest, approximately 4,388 ppmv, followed by 1,047 ppmv in the TSC and 746 ppmv in the GAC. The spring water pCO_2 in the BZC showed a drastic increasing trend during the growing season from January to September, with an amplitude of around 6,000 ppmv, whereas the pH and SI_c values showed a reverse seasonal cycle with peaks occurring in January (Fig. 3b). In contrast, the pCO_2 in the TSC showed a different seasonal variation from that in the BZC, with an amplitude below 1,000 ppmv. The highest pCO_2 in the TSC occurred in winter, between January and April (Fig. 3c). For the GAC, the pCO_2 showed only minor seasonal variations throughout the study period, with an average of around 700 ppmv (Fig. 3a).

Distinctive HCO_3^- cycles were found in all catchments. In the GAC, the lowest [HCO_3^-] occurred between May and July (~100 mg L^{-1}), and [HCO_3^-] then increased gradually, reaching a maximum between January and March (Fig. 3a). The [HCO_3^-] in the TSC experienced strong gradients occurring in April and October—for instance, in October 2007, the [HCO_3^-] showed an increase of approximately 70 mg L^{-1} in one month and sustained high values until it drastically declined to the original level in April 2008 (Fig. 3c). The [HCO_3^-] in the BZC showed a different seasonal change pattern from the two alpine catchments and experienced an increasing [HCO_3^-] trend from January to September. At the end of September, [HCO_3^-] started to drop and then reached the lowest value between April and May (Fig. 3b).

Discharge in the three catchments was generally lower in winter, whereas the highest water flow occurred between June and July. The TSC showed a unique hydrological pattern because of the impact of the glacier (Fig. 1c). When the average air temperature rose above 10 °C, the equilibrium line reached the glacier front in the TSC and the glacier started to melt, leading to higher discharge from mid-July to November (Zeng

et al. 2012). Note that discharge in the GAC showed a pattern with peaks following rainfall and clearly pronounced recession limbs. The BZC, in contrast, showed large peaks in discharge and only short recession limbs.

The calculated CCSF for the three catchments was mainly dominated by variations in discharge, which in turn were dominated by the seasonal cycles. Through the whole study period, the GAC had the highest average CCSF, nearly 59.96 t CO_2 km^{-2} $year^{-1}$ (or 16.35 t C km^{-2} $year^{-1}$), followed by the TSC with an average of 54.18 t CO_2 km^{-2} $year^{-1}$ (or 14.78 t C km^{-2} $year^{-1}$; Zeng et al. 2012), and the BZC with an average of 23.77 t CO_2 km^{-2} $year^{-1}$ (or 6.48 t C km^{-2} $year^{-1}$; Zeng et al. 2016; Table 1).

Diurnal variations in physicochemical parameters during 4-day dry periods

The physicochemical parameters associated with 4-day dry periods during a summer period (between June and August) and a winter period (between December and February) are shown in Figs. 4 and 5, respectively. Each value in Figs. 4 and 5 was plotted or calculated over a continuous 96-h period (4 days) to present the dynamics of carbonate weathering in diurnal cycles.

The measured water temperatures in the GAC showed a clear diurnal cycle. However, this cycle had nothing to do with temperature variations in the aquifer but reflected the direct influence of air temperature on water temperature at the measurement point. No significant diurnal water temperature cycles (<0.1 °C) were observed in the BZC or TSC.

In summer, the pH in the TSC peaked at night between 10 PM and 6 AM (Fig. 4c), whereas no considerable pH variations (<0.1) were found in winter (Fig. 5c). The most variable diurnal pCO_2 cycle occurred in the TSC during summer, with values approximately 400 ppmv higher in the late afternoon than in the early morning (Fig. 4c). There were fewer diurnal changes in pCO_2 in the BZC and GAC observed in the same period (Fig. 4a,b).

Clear diurnal cycles were found in HCO_3^- concentrations in the GAC and TSC. The [HCO_3^-] in the GAC reached a minimum between noon and 2 PM, whereas peaks occurred at around 9 PM (T1–T4 in Fig. 4a). This was most likely a direct effect of the temperature variations at the measurement point as shown above, which had nothing to do with [HCO_3^-] variations in the aquifer. In the TSC, the maximum [HCO_3^-] occurred at 6 PM, whereas the lowest [HCO_3^-] appeared in the early morning (Fig. 4c). The discharge showed diurnal change in the TSC in summer, reaching the maximum at 6 PM (F1–F4 in Fig. 4c). The [HCO_3^-] in the BZC showed no clear diurnal oscillation during the same period (Fig. 4b).

Again, the CCSF showed a highly relevant correlation with discharge in the daily cycles. Compared with all the records in summer, less remarkable daily changes were found in most parameters in the GAC, BZC, and TSC in the winter period (cf. Figs. 4 and 5).

Short-term variations in physicochemical parameters during storm events

Figure 6 shows the typical changes in physicochemical parameters during storm events in the three catchments in summer seasons (accumulated precipitation of around 105 mm in the GAC, 198 mm in the BZC, and 24 mm in the TSC). Clearly, the water pCO_2, SI_c, and [HCO_3^-] generally declined as the discharge increased during heavy rainfall and then returned to the original level after the storms. However, the CCSF still showed synchronous in-phase change with discharge (Fig. 6).

Discussion

Control of climate on carbonate weathering in alpine karst catchments

Temperature increase causes decreasing carbonate dissolution, which has been observed in laboratory experiments (Dreybrodt 1988). It limits the solubility of $CaCO_3$; which means that there is lower equilibrium concentration of HCO_3^- when the temperature increases. This behavior is based on the assumption that pCO_2 is fixed.

In the GAC, the calculated water pCO_2 varied by only 1,100 ppmv (400–1,500 ppm, Fig. 3a), showing little difference between summer and winter because of the lower vegetation cover in its recharge area. The seasonal fluctuation of the water temperature in the GAC was approximately 10 °C, but shows the direct impact of air temperature at this measurement site, as shown previously. The real water temperature variation in the GAC could be small, similar to that in the TSC as shown below. Thus, the seasonal [HCO_3^-] cycles were controlled mainly by the dilution effect. The considerable SI_c decline in the GAC occurred during the snow-melting season from April to June and storm events during May and July (Fig. 3a) because of the dilution effect.

There was almost no seasonal water temperature change (<0.5 °C) in the TSC; moreover, there was little vegetation development in the recharge area (Fig. 1c). Therefore, the [HCO_3^-] change in the TSC for the entire study period depended mainly on the flow change; in other words, it was controlled by the dilution effect through increased discharge (Liu et al. 2007; Zeng et al. 2012). The higher discharge in the snow/ice-melting period diluted the water in the wet season, and therefore the [HCO_3^-] and pCO_2 values decreased. In contrast, the low water flow in the freezing season caused a

Table 1 Statistics on temporal variations of the hydrological and hydrochemical parameters of the three catchments (*GAC*, *BZC* and *TSC*)

Parameter	Statistic	Catchment		
		Gadenalpe (GAC)	Banzhai (BZC)	Tsanfleuron-Sanetsch (TSC)
Discharge (L s^{-1})	Average	227.83	199.63	529.76
	CV[e]	0.95	4.52	0.99
	N[f]	13,693	72,384	26,038
Runoff depth (m $year^{-1}$)	Average	1.17	0.33	1.52
	CV	–	–	–
	N	–	–	–
Water temperature (°C)	Average	4.41	18.40	4.25
	CV	0.39	0.03	0.06
	N	13,693	72,384	26,038
pH	Average	8.19	7.59	8.02
	CV	0.01	0.03	0.02
	N	13,693	72,384	26,038
SI_c[a]	Average	0.09	0.25	0.07
	CV	–	–	–
	N	–	–	–
SI_d[b]	Average	−0.17	0.025	−2.46
	CV	–	–	–
	N	–	–	–
pCO_2 (ppmv)[c]	Average	745.94	4387.52	1047.62
	CV	0.21	0.44	0.38
	N	13,693	72,384	26,038
HCO_3^- (mg L^{-1})	Average	154.34	222.70	134.19
	CV	0.14	0.09	0.31
	N	13,693	72,384	26,038
CCSF (t CO_2 km^{-2} $year^{-1}$)[d]	Average	59.96	23.77	54.18
	CV	0.84	4.26	0.81
	N	13,693	72,384	26,038

[a] Saturation index of calcite

[b] Saturation index of dolomite

[c] pCO_2 partial pressure of water

[d] Carbon sink fluxes by carbonate weathering

[e] Coefficient of variation = standard deviation/mean

[f] Number of records

sharp increase in $[HCO_3^-]$ (Fig. 3c). The SI_c variations in the TSC further confirmed this dilution effect. A rapid decline in SI_c by nearly 1 unit was found at the transition point from the dry season to the wet season in the TSC (+0.5 to −0.5, Fig. 3c).

Control of land cover on carbonate weathering in the subtropical catchment

The role of temperature in carbonate weathering is more complex in subtropical catchments. It is widely accepted that temperature acts as a fundamental promoting factor for soil respiration (e.g., Bond-Lamberty and Thomson 2010). The vegetation ecosystem responds sensitively to the seasonal temperature cycle, showing differences in biotic productivity throughout the year. Thus, the development of the vegetation ecosystem controls carbonate weathering in another way, promoting dissolution by enhancing soil respiration (increasing the pCO_2 level at the soil–rock interface; Romero-Mujalli et al. 2019b). The BZC, covered mostly with natural forest (95%) and dominated by a warm and humid climate, is an ideal site to contrast with the alpine sites of the GAC and TSC, where less soil/vegetation is developed because of the alpine climate. It was suggested that the high proportion of vegetation cover may significantly contribute to hydrochemical variations in the BZC. The role of air temperature here was positively

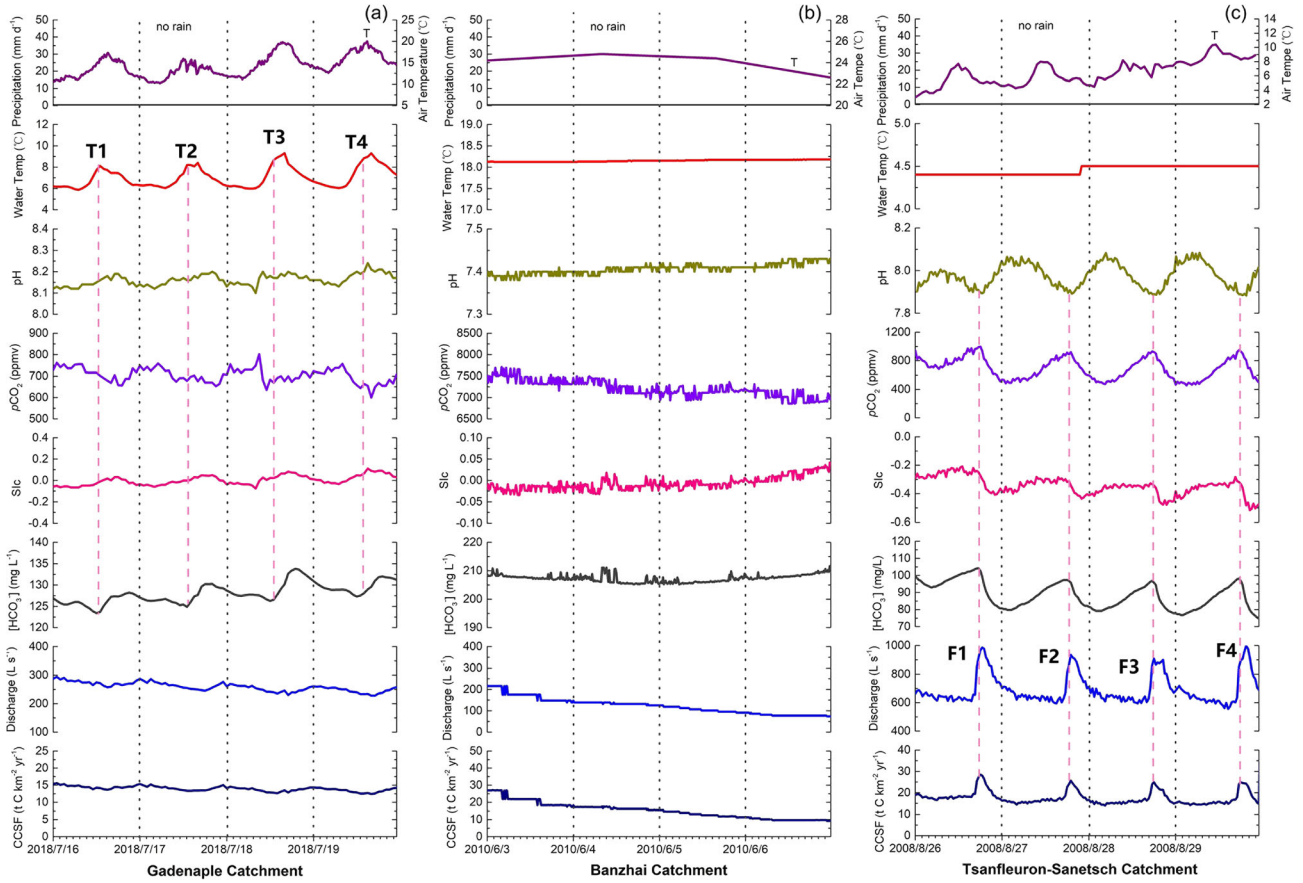

Fig. 4 Diurnal variations during a dry period in summer for air temperature, precipitation, discharge, water temperature, pH, calculated $[HCO_3^-]$, pCO_2, SI_c, and carbonate-weathering carbon sink flux (CCSF) in **a** the Gadenalpe Catchment (GAC), **b** the Banzhai Catchment (BZC), and **c** the Tsanfleuron-Sanetsch Catchment (TSC). The dashed lines are the splitting points of each day (0:00). F1–F4: points with a strong dilution effect. T1–T4: points with a strong temperature effect. Note: The water temperature variations in the GAC are an artifact, because the measurement point is about 200–300 m below the spring outlets due to inaccessibility of the outlets

correlated with carbonate weathering by promoting soil respiration and thus increasing the system pCO_2. The forest cover in the BZC (Fig. 2b) led to considerable seasonal changes in pCO_2 and $[HCO_3^-]$ (Fig. 3b), differing from those in the GAC and TSC, where soil/vegetation systems are absent in the recharge areas (Fig. 1a,c). From January to September, as the air temperature increased, soil respiration increased gradually in in BZC and peaked during September (Fig. 3b). During this period, water pCO_2 increased from 1,435 to 13,614 ppmv, an almost nine-fold increase, and $[HCO_3^-]$ increased from 190 to 328 mg L^{-1} (a 138 mg L^{-1} increase), close to the theoretical calculation of $[HCO_3^-]$ increase of 132 mg L^{-1}. Therefore, in the BZC, it was the seasonal pCO_2 variation that resulted in the largest change in $[HCO_3^-]$ concentration. To conclude, the BZC is an ideal site to show the dominant role of the vegetation ecosystem over temperature in carbonate weathering; that is, the positive effect by the vegetation ecosystem overtook the negative impact caused by temperature change (seasonal water temperature varied only 2 °C in the BZC, Fig. 3b).

Quantifying the counterbalancing effects of temperature and ecosystem production on carbonate weathering

Here, a modeling perspective to estimate the required pCO_2 for each degree of temperature increase was developed based on the thermodynamics of calcite and dolomite dissolution, respectively, for two fixed equilibrium DIC (HCO_3^-) concentrations (2 and 4 mmol L^{-1}, covering the $[HCO_3^-]$ range for the three catchments) across a wide range of annual mean temperatures from 0 to 30 °C (dashed lines in Fig. 7a). It was found that the pCO_2 to sustain a constant $[HCO_3^-]_{eq}$ at 30 °C was about 8.3 times higher than that at 0 °C. This means that when the environment becomes over-heated, the impact of every CO_2 molecule increase becomes less important to $[HCO_3^-]_{eq}$.

As mentioned previously, substantial seasonal variations in pCO_2 and $[HCO_3^-]_{eq}$ may mainly be attributed to seasonal change in the vegetation ecosystem's productivity and its ecological response to seasonal temperature change. To simplify the relation between temperature and pCO_2 or $[HCO_3^-]_{eq}$

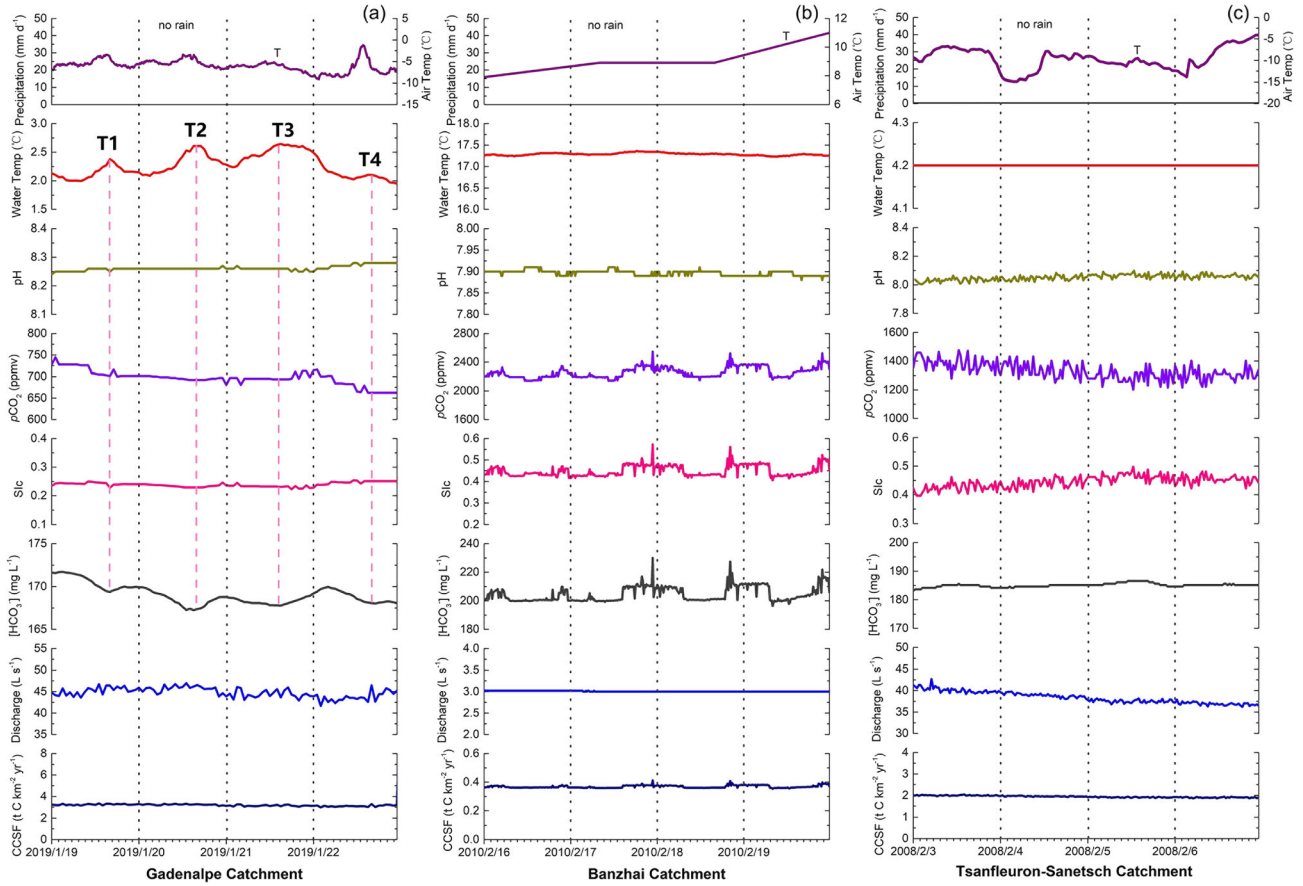

Fig. 5 Diurnal variations during a dry period in winter for air temperature, precipitation, discharge, water temperature, pH, calculated [HCO_3^-], pCO_2, SI_c, and carbonate-weathering carbon sink flux (CCSF) in **a** the Gadenalpe Catchment (GAC), **b** the Banzhai Catchment (BZC), and **c** the Tsanfleuron-Sanetsch Catchment (TSC). The dashed lines are the splitting points of each day (0:00). T1–T4: points with a strong temperature effect. Note: The water temperature variations in the GAC are an artifact, because the measurement point is about 200–300 m below the spring outlets due to inaccessibility of the outlets

under vegetation cover, three temperature-based soil CO_2 ecological models by Romero-Mujalli et al. (2019b) were used. As shown in Fig. 7a, the soil CO_2 may experience exponential increase with temperature when the annual temperature is below ~15 °C (see solid lines in Fig. 7a). The increasing soil CO_2 trend will be highly constrained if the temperature surpasses the optimum temperature for ecosystem respiration (Romero-Mujalli et al. 2019b). However, the negative impact of temperature on carbonate solubility is unchanged (Dreybrodt 1988). Because there exists a counterbalancing effect of thermodynamics and ecosystem production on carbonate weathering, three $[HCO_3^-]_{eq}$ (DIC) unimodal curves were obtained after accounting for changes of the vegetation ecosystem, with the DIC concentration reaching the maximum at about 15 °C (Romero-Mujalli et al. 2019b), as shown in Fig. 7b (see solid lines). In the present study in the BZC, the findings of this study further verified that this counterbalancing effect may even occur in the seasonal cycles of DIC (Fig. 3b). However, it is stressed that this seasonal control of temperature may only occur in a system with soil/vegetation development. This means that vegetation ecosystem productivity must be strongly related to the seasonal air temperature change, as evidenced in the BZC (Fig. 3b). In contrast, the data for the GAC exhibited a different behavior. Because of the absence of vegetation (and thus less seasonal pCO_2 change in Fig. 3a) in the GAC, the seasonal dilution effect may account for most [HCO_3^-] changes (Fig. 3a). In addition, in the GAC, as the water temperature peaked during mid-day, the [HCO_3^-] dropped to the lowest level (T1–T4 in Figs. 4a and 5a), although the spring water temperature might have been stable. The lowest water temperatures in the freezing season resulted in the highest DIC concentrations (Fig. 3a). The temperature impact and the role of the vegetation ecosystem were also found in the previous study at the Shawan Karst Test Site (Zeng et al. 2017). Bare rock and bare soil cover showed less or reverse [HCO_3^-] variations compared with vegetated lands. Lush vegetation resulted in higher [HCO_3^-] concentrations in summer (Zeng et al. 2017). Thus, it is stressed that the counterbalancing effect will only be effective in a vegetation ecosystem. The temperature effect may be more significant if vegetation cover is absent. Therefore, it is suggested that land-use and land-cover change is a

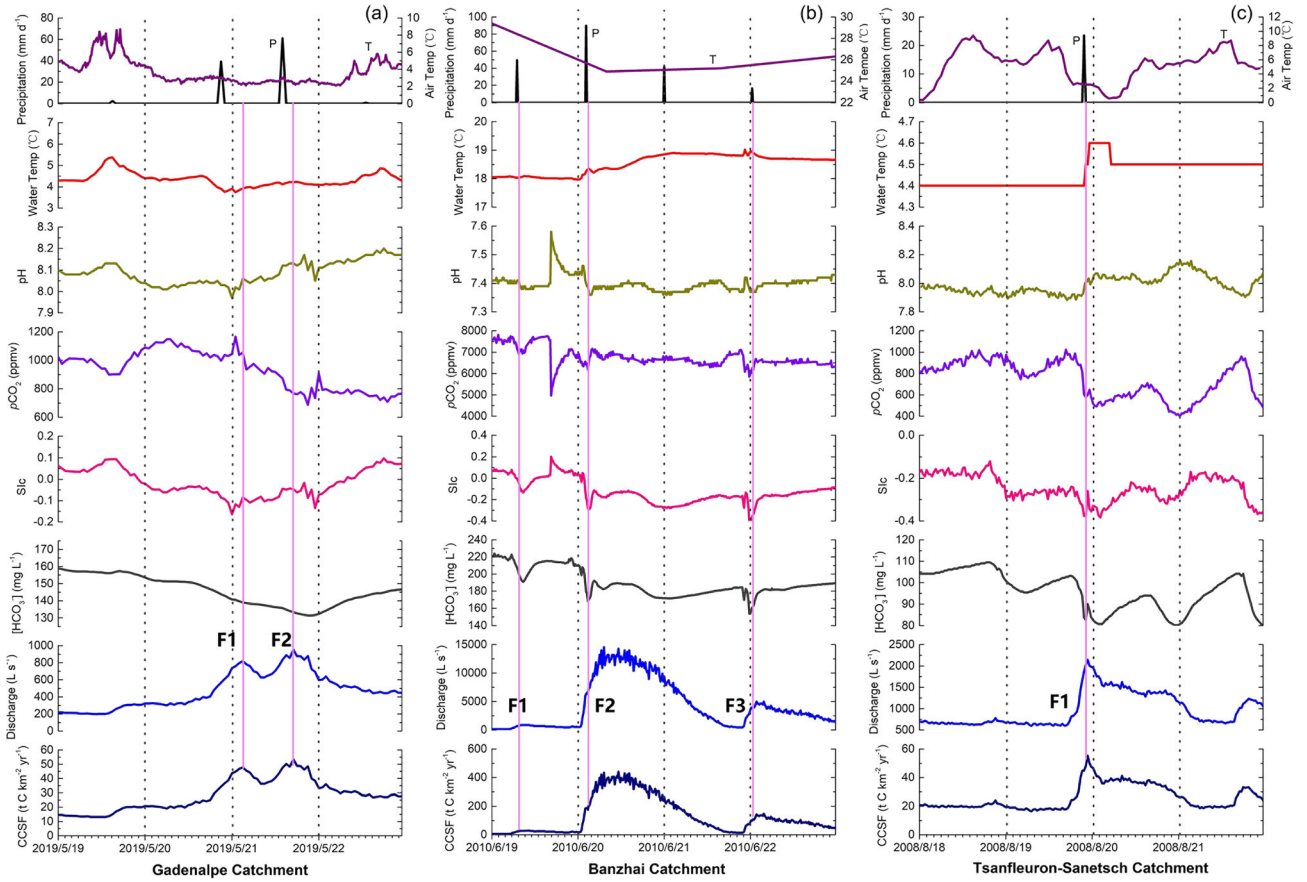

Fig. 6 Short-term variations during a storm event for air temperature, precipitation, discharge, water temperature, pH, calculated [HCO_3^-], pCO_2, SI_c, and carbonate-weathering carbon sink flux (CCSF) in **a** the Gadenalpe Catchment (GAC), **b** the Banzhai Catchment (BZC), and **c** the Tsanfleuron-Sanetsch Catchment (TSC) during rain-storm periods. F1–F3: points with a strong dilution effect

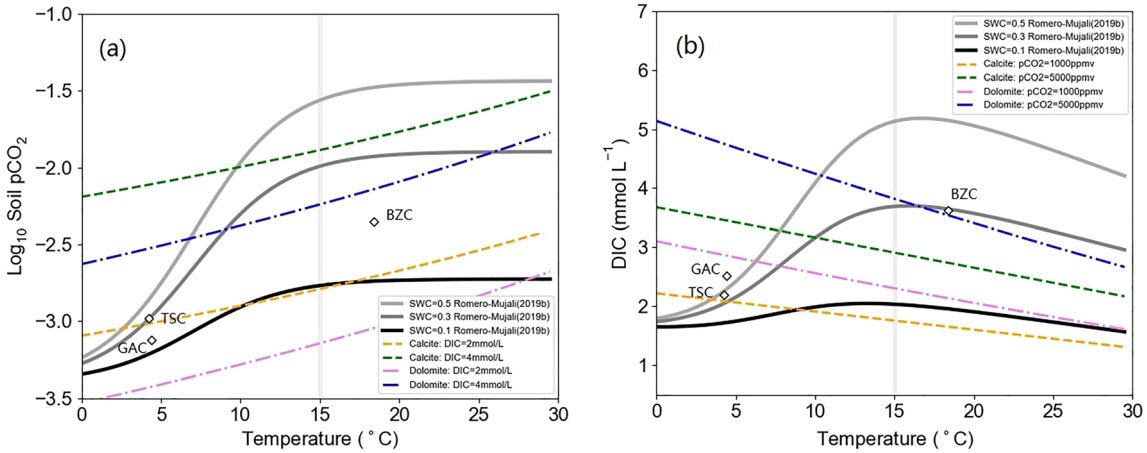

Fig. 7 **a** The required pCO_2 (dashed lines) based on the thermodynamics of calcite and dolomite dissolution, respectively, at two fixed equilibrium DIC (HCO_3^-) concentrations (2 and 4 mmol L^{-1}, covering the DIC range for the three catchments) across a wide range of annual mean temperatures from 0 to 30 °C and the three predicted pCO_2 values (solid lines) by Romero-Mujalli et al. (2019b), considering soil water content (SWC) as a function of temperature. **b** The equilibrium DIC concentration as a function of temperature. The equilibrium DIC concentration at the three predicted soil pCO_2 values (solid lines) show a decreasing trend when the temperature is higher than 15 °C. The DIC concentrations at the two fixed soil pCO_2 values (500 and 5,000 ppmv, covering the pCO_2 change for the three catchments, dashed lines) show a decreasing trend as the temperature increases because of the negative thermodynamic impact on calcite and dolomite dissolution, respectively

significant factor that needs to be considered in global carbonate weathering models (Zeng et al. 2019). Goldscheider (2019) also emphasized that healthy soils and vegetation increase the efficiency of CO_2 sinks, contribute to natural groundwater protection, and help to sustain surface and subsurface biodiversity in karst systems.

Runoff dominates carbonate-weathering carbon sink flux

Water flow is a fundamental driver for CCSF (Hartmann 2009; Moosdorf et al. 2011; Zeng et al. 2016; Zeng et al. 2019). Hydrological events in wet seasons may strongly affect the concentration and saturation state through large amounts of inflowing freshwater, which influence the solute flux. For instance, pCO_2 was the highest from June to July in the BZC in 2010 (Fig. 3b). However, the elevated water flow sharply diluted the [HCO_3^-] in this period (F1–F3 in Fig. 6b); the highest concentration was delayed and occurred in November (Fig. 3b). The GAC showed a similar [HCO_3^-] decrease during the snow-melting period and storm events between April and June (Fig. 3a). The most significant dilution effect was in the TSC (F–F4 in Fig. 4c, F1 in Fig. 6c), which was charged by three water sources during summer: glacier melting, snow melting, and rainfall (Zeng et al. 2012). The impact of fluctuating water flow on [HCO_3^-] variation was overwhelming through the whole study period (Fig. 3c). Although the increased water flow during these hydrological events considerably reduced the DIC concentration, it failed to alter the highly positive correlation between runoff and CCSF at both the seasonal and diurnal scales. As shown in Fig. 8a, a strong linear correlation between runoff and CCSF in all the three catchments was found. These results were attributed to what is called the chemo-static behavior of carbonate weathering, which has been found in numerous studies (Godsey et al. 2009; Zeng et al. 2016). The BZC had the highest proportion of vegetation cover and the largest catchment area (~19 km^2). Therefore, its strongest soil respiration and possible longer reaction time resulted in the most prominent chemo-static behavior (the gentlest [HCO_3^-] decrease with runoff in Fig. 8c) and the highest linear correlation coefficient between runoff and CCSF (Fig. 8a). In summary, runoff dominated the carbonate-weathering carbon sink flux in all three karst catchments.

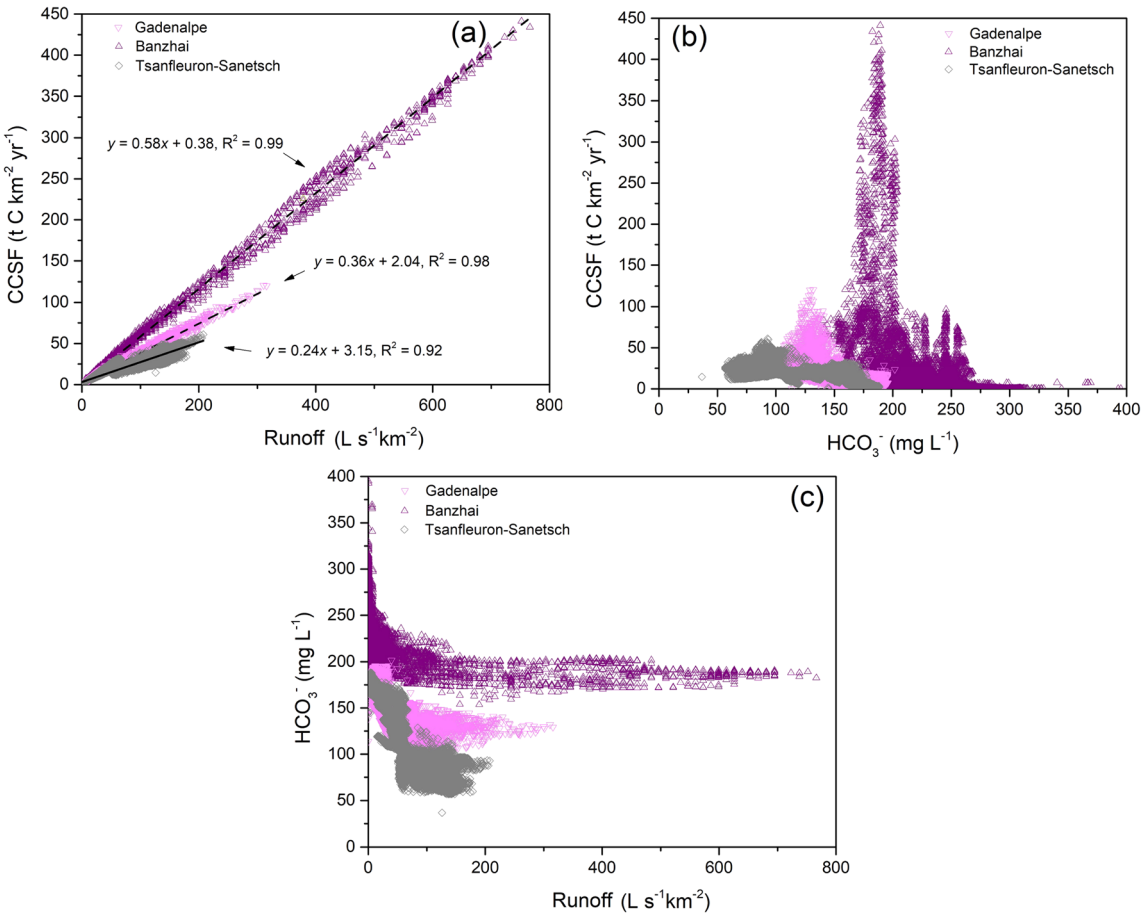

Fig. 8 **a** Relationships between carbonate-weathering carbon sink flux (CCSF) and runoff, **b** relationships between CCSF and HCO_3^- concentration, and **c** relationships between [HCO_3^-] and runoff in the three studied karst catchments (GAC, BZC, and TSC)

Implications for future carbonate weathering research

In previous global carbonate weathering intensity models, temperature, evapotranspiration, and/or water soil content were considered as a single or dual parameter for soil pCO_2 (Brook et al. 1983; Gaillardet et al. 2019; Romero-Mujalli et al. 2019b). It is suggested that these assumptions may underestimate the role of different land covers. The soil biota productivities of different vegetation types may have more significant impacts on soil pCO_2 and carbonate dissolution than other factors (Zeng et al. 2017). Moreover, the factors controlling the primary production or soil respiration of a specific ecosystem may also be numerous (Del Grosso et al. 2008; Hibbard et al. 2005; Thomey et al. 2011). A climate sensitive zone may not fit all types of ecosystem or land use. In addition, many constructed carbonate weathering intensity models rely on numerous individual field DIC observations, which may show highly scattered sampling times or preferred sampling months. However, the present findings confirmed that different land uses may result in considerably different seasonal [HCO_3^-] patterns because of the coupled effect of temperature and the ecosystem. Thus, the seasonal variations of [HCO_3^-] need to be considered in future field sampling strategies. More importantly, global climate and land-use changes will be essential factors to consider in the future. A better understanding and accurate estimation of the carbonate weathering behavior in different ecosystems are necessary for us to predict CCSF changes.

In addition, the CCSF is controlled by both discharge and DIC concentration. As showed above, runoff changes dominated the CCSF change in all situations. Nonforest/soil or bare rock terrain may also lead to greater bicarbonate export because of lower evapotranspiration (Zeng et al. 2016; Zeng et al. 2017). The CCSF in the GAC and TSC alpine catchments was nearly 2.5 times higher than that in the BZC subtropical catchment, although strong soil respiration generated the highest DIC concentration in the BZC. The large water loss via evapotranspiration in vegetated land may have a negative impact on CCSF. In conclusion, the occurrence of a vegetation ecosystem complicates carbonate weathering and the carbon sink flux produced by this chemical process. More efforts are still needed to further unveil the mechanisms behind this phenomenon.

Conclusions

To gain a better understanding of carbonate weathering under climate and land-use changes, this study compared and analyzed high-frequency hydrochemical data from study sites in the GAC (Austrian Alps), TSC (Swiss Alps), and BZC (Southwest China). The added value of this study is the systematic comparison of these three contrasting karst catchments, which allowed differentiation of the effects of air temperature, runoff, and land-cover on carbonate weathering and the atmospheric CO_2 sink. The results demonstrated that in the two alpine carbonate catchments (the GAC and TSC), the small proportions of vegetation cover (20–39%) and low temperatures limited soil respiration, thereby producing lower pCO_2 values. For this reason, the dilution effect, which is strongly influenced by the influence of air temperature on freezing and thawing, determined the seasonal and/or short-term change of [HCO_3^-], resulting in a lower [HCO_3^-] concentration during high-flow periods in the warm season, which included snowmelt, glacier melt (in the TSC), and precipitation events. In contrast, a different pattern of seasonal [HCO_3^-] change could be found in the subtropical catchment (the BZC) covered by 95% natural forest. In the BZC, because of the active vegetation of the ecosystem, the seasonal [HCO_3^-] change was mainly attributed to the large seasonal fluctuation of pCO_2. The strong productivity of the soil biota in summer and autumn resulted in the highest [HCO_3^-] in the BZC. The [HCO_3^-] in the forested catchment was 40–60% higher than that in the alpine catchments. However, the periodic snow and/or ice-melting water supplies and lower evapotranspiration in the GAC and TSC resulted in higher CCSF. This elevated CCSF in the alpine catchments can be attributed to the chemo-static behavior of carbonate weathering and the dominance of runoff/discharge in determining the CCSF. Based on the equilibrium modeling perspective for a global temperature range, it is suggested that the role of soil pCO_2 increase is crucial for carbonate dissolution in low-temperature zones (<15 °C). In higher-temperature environments (>15 °C), the high temperature may constrain both the solubility of carbonate and the productivity of the vegetation ecosystem. It is stressed that the vegetation ecosystem alters the role of temperature in carbonate weathering, from a one-way negative temperature impact in bare-rock landscapes to a counterbalancing effect of temperature and ecosystem production on carbonate weathering in vegetated karst catchments. It is predicted that under future global warming, karst regions in cold climates will have increasing CO_2 consumption potential, whereas karst regions in warm climates (>15 °C) will have decreasing CO_2 consumption potential, particularly when precipitation decreases at the same time. To conclude, ecosystem function is significant, and its influences need to be further quantified in future carbonate weathering research.

Funding information This work was supported by the Strategic Priority Research Program of the Chinese Academy of Sciences (grant number XDB 40020000) and the National Natural Science Foundation of China (grant numbers U1612441 and 41921004).

Compliance with ethical standards

Declaration of Competing Interest The authors declare that they have no known competing financial interests or personal relationships that could have influenced the work reported in this paper.

References

Adams JM, Post WM (1999) A preliminary estimate of changing calcrete carbon storage on land since the Last Glacial Maximum. Glob Planet Chang 20(4):243–256

Beaulieu E, Goddéris Y, Donnadieu Y, Labat D, Roelandt C (2012) High sensitivity of the continental-weathering carbon dioxide sink to future climate change. Nature Clim Change 2:46–349

Bond-Lamberty B, Thomson A (2010) Temperature-associated increases in the global soil respiration record. Nature 464:579–582

Brook GA, Folkoff ME, Box EO (1983) A world model of soil carbon dioxide. Earth Surf Process Landf 8(1):79–88

Del Grosso S, Parton W, Stohlgren T, Zheng DL, Bachelet D, Prince S, Hibbard K, Olson R (2008) Global potential net primary production predicted from vegetation class, precipitation, and temperature. Ecology 89(8):2117–2126

Dreybrodt W (1988) Processes in karst systems. Springer, Heidelberg, Germany

Faust K (2017) Dynamik hydrochemischer parameter von Karstquellen und Gewässern im Gadental (Österreich) unter besonderer Berücksichtigung von Wasserhaushaltsprozessen [Dynamics of hydrochemical parameters of karst springs and waters in the Gadental (Austria) with special consideration of water balance processes]. MSc Thesis, KIT, Germany

Gaillardet J, Calmels D, Romero-Mujalli GZ, Zakharova E, Hartmann J (2019) Global climate control on carbonate weathering intensity. Chem Geol 527:118762

Gislason SR, Oelkers EH, Eiriksdottir ES, Kardjilov MI, Gisladottir G, Sigfusson B, Snorranson A, Elefsen S, Hardardottir J, Torssander P, Oskarsson N (2009) Direct evidence of the feedback between climate and weathering. Earth Planet Sci Lett 277(1–2):213–222

Goddéris Y, Williams JZ, Schott J, Pollard D, Brantley SL (2010) Time evolution of the mineralogical composition of Mississippi Valley loess over the last 10 kyr: climate and geochemical modelling. Geochim Cosmochim Acta 74(22):6357–6374

Godsey SE, Kirchner JW, Clow DW (2009) Concentration-discharge relationships reflect chemostatic characteristics of US catchments. Hydrol Proc 23(13):1844–1864

Goldscheider N (2019) A holistic approach to groundwater protection and ecosystem services in karst terrains. Carbon Evapor 34:1241–1249

Goldscheider N, Chen Z, Broda S, Auler AS, Bakalowicz M, Drew D, Hartmann J, Jiang G, Moosdorf N, Stevanovic Z, Veni G (2020) Global distribution of carbonate rocks and karst water resources. Hydrogeol J. https://doi.org/10.1007/s10040-020-02139-5

Gremaud V, Goldscheider N, Savoy L, Favre G, Masson H (2009) Geological structure, recharge processes and underground drainage of a glacierised karst aquifer system, Tsanfleuron-Sanetsch, Swiss Alps. Hydrogeol J 17:1833–1848

Gremaud V, Goldscheider N (2010) Geometry and drainage of a retreating glacier overlying and recharging a karst aquifer, Tsanfleuron–Sanetsch, Swiss Alps. Acta Carsol 39:289–300

Gwiazda RH, Broecker WS (1994) The separate and combined effects of temperature, soil pCO_2 and organic acidity on silicate weathering in the soil environment: formulation of a model and results. Global Biogeochem Cy 8(2):141–155

Haberl H, Erb KH, Krausmann F, Gaube V, Bondeau A, Plutzar C, Gingrich S, Lucht W, Fischer-Kowalski M (2007) Quantifying and mapping the human appropriation of net primary production in Earth's terrestrial ecosystems. Proc Natl Acad Sci 104(31):12942–12947

Hartmann J (2009) Bicarbonate-fluxes and CO_2-consumption by chemical weathering on the Japanese archipelago: application of a multi-lithological model framework. Chem Geol 265(3–4):237–271

Hibbard KA, Law BE, Reichstein M, Sulzman J (2005) An analysis of soil respiration across northern hemisphere temperate ecosystems. Biogeochemistry 73:29–70

Liu Z, Zhao J (2000) Contribution of carbonate rock weathering to the atmospheric CO_2 sink. Environ Geol 39:1053–1058

Liu Z, Li Q, Wang J (2007) Seasonal, diurnal and storm-scale hydrochemical variations of typical epikarst springs in subtropical karst areas of SW China: soil CO_2 and dilution effects. J Hydrol 337(1–2):207–223

Liu Z, Dreybrodt W, Wang H (2010) A new direction in effective accounting for the atmospheric CO_2 budget: considering the combined action of carbonate dissolution, the global water cycle and photosynthetic uptake of DIC by aquatic organisms. Earth Sci Rev 99(3–4):162–172

Liu Z, Dreybrodt W, Liu H (2011) Atmospheric CO_2 sink: silicate weathering or carbonate weathering? Appl Geochem 26:292–294

Liu Z, Macpherson GL, Groves C, Martin JB, Yuan D, Zeng S (2018) Large and active CO_2 uptake by coupled carbonate weathering. Earth Sci Rev 182:42–49

Macpherson GL, Sullivan PL, Stotler RL, Norwood BS (2019) Increasing groundwater CO_2 in a mid-continent tallgrass prairie: controlling factors. E3S Web Conf 98:06008. https://doi.org/10.1051/e3sconf/20199806008

Martin JB (2017) Carbonate minerals in the global carbon cycle. Chem Geol 449:58–72

Moosdorf N, Hartmann J, Lauerwald R, Hagedorn B, Kempe S (2011) Atmospheric CO_2 consumption by chemical weathering in North America. Geochim Cosmochim Acta 75(24):7829–7854

Raymond PA, Hamilton SK (2018) Anthropogenic influences on riverine fluxes of dissolved inorganic carbon to the oceans. Limnol Oceanogr Lett 3(3):141–155

Raymond PA, Oh NH, Turner RE, Broussard W (2008) Anthropogenically enhanced fluxes of water and carbon from the Mississippi River. Nature 451:449–452

Riebesell U, Schulz KG, Bellerby RGJ, Botros M, Fritsche P, Meyerhoefer M, Neill C, Nondal G, Oschlies A, Wohlers J, Zöellner E (2007) Enhanced biological carbon consumption in a high CO_2 ocean. Nature 450:545–548

Romero-Mujalli GJ, Hartmann B, Boerker J (2019a) Temperature and CO_2 dependency of global carbonate weathering fluxes: implications for future carbonate weathering research. Chem Geol 527:118874

Romero-Mujalli G, Hartmann J, Borker J, Gaillardet J, Calmels D (2019b) Ecosystem controlled soil-rock pCO_2 and carbonate weathering: constraints by temperature and soil water content. Chem Geol 527:118634

Sheng H, Yang Y, Yang Z, Chen G, Xie J, Guo J, Zou S (2010) The dynamic response of soil respiration to land use changes in subtropical China. Glob Chang Biol 16(3):1007–1121

Thomey ML, Collins SL, Vargas R, Johnson JE, Brown RF, Natvig DO, Friggens MT (2011) Effect of precipitation variability on net primary production and soil respiration in a Chihuahuan Desert grassland. Glob Chang Biol 17(4):1505–1515

Wigley TML (1977) WATSPEC: a computer program for determining equilibrium speciation of aqueous solutions. British Geomorphological Research Group, London, pp 1–48

Zeng C, Gremaud V, Zeng H, Liu Z, Goldscheider N (2012) Temperature-driven meltwater production and hydrochemical

variations at a glaciated alpine karst aquifer: implication for the atmospheric CO_2 sink under global warming. Environ Earth Sci 65:2285–2297

Zeng C, Liu Z, Zhao M, Yang R (2016) Hydrologically-driven variations in the karst-related carbon sink fluxes: insights from high-resolution monitoring of three karst catchments in Southwest China. J Hydrol 533:74–90

Zeng Q, Liu Z, Chen B, Hu Y, Zeng S, Zeng C, Yang R, He H, Zhu H, Cai X, Chen J, Ou Y (2017) Carbonate weathering-related carbon sink fluxes under different land uses: a case study from the Shawan Simulation Test Site, Puding, Southwest China. Chem Geol 474:58–71

Zeng S, Liu Z, Kaufmann G (2019) Sensitivity of the global carbonate weathering carbon-sink flux to climate and land-use changes. Nat Commun 10:5749